



RESEARCH ARTICLE

Disruption of the NlpD lipoprotein of the plague pathogen *Yersinia pestis* affects iron acquisition and the activity of the twin-arginine translocation system

Avital Tidhar *, Yinon Levy, Ayelet Zauberman, Yaron Vagima, David Gur, Moshe Aftalion, Ofir Israeli , Theodor Chitlaru, Naomi Ariel, Yehuda Flashner, Anat Zvi, Emanuelle Mamroud *

Department of Biochemistry and Molecular Genetics, Israel Institute for Biological Research, Ness-Ziona, Israel

* avitalt@iibr.gov.il (AT); emmym@iibr.gov.il (EM)



 OPEN ACCESS

Citation: Tidhar A, Levy Y, Zauberman A, Vagima Y, Gur D, Aftalion M, et al. (2019) Disruption of the NlpD lipoprotein of the plague pathogen *Yersinia pestis* affects iron acquisition and the activity of the twin-arginine translocation system. PLoS Negl Trop Dis 13(6): e0007449. <https://doi.org/10.1371/journal.pntd.0007449>

Editor: Abdallah M. Samy, Faculty of Science, Ain Shams University (ASU), EGYPT

Received: October 17, 2018

Accepted: May 8, 2019

Published: June 6, 2019

Copyright: © 2019 Tidhar et al. This is an open access article distributed under the terms of the [Creative Commons Attribution License](https://creativecommons.org/licenses/by/4.0/), which permits unrestricted use, distribution, and reproduction in any medium, provided the original author and source are credited.

Data Availability Statement: The transcriptome results are available online (<http://www.ncbi.nlm.nih.gov/geo/>, record GSE101490).

Funding: This project has been supported by funds from the Israel Institute for Biological Research, SB-5112-181. The funders had no role in study design, data collection and analysis, decision to publish, or preparation of the manuscript.

Competing interests: The authors have declared that no competing interests exist.

Abstract

We have previously shown that the cell morphogenesis NlpD lipoprotein is essential for virulence of the plague bacteria, *Yersinia pestis*. To elucidate the role of NlpD in *Y. pestis* pathogenicity, we conducted a whole-genome comparative transcriptome analysis of the wild-type *Y. pestis* strain and an *nlpD* mutant under conditions mimicking early stages of infection. The analysis suggested that NlpD is involved in three phenomena: (i) Envelope stability/integrity evidenced by compensatory up-regulation of the Cpx and Psp membrane stress-response systems in the mutant; (ii) iron acquisition, supported by modulation of iron metabolism genes and by limited growth in iron-deprived medium; (iii) activity of the twin-arginine (Tat) system, which translocates folded proteins across the cytoplasmic membrane. Virulence studies of *Y. pestis* strains mutated in individual Tat components clearly indicated that the Tat system is central in *Y. pestis* pathogenicity and substantiated the assumption that NlpD essentiality in iron utilization involves the activity of the Tat system. This study reveals a new role for NlpD in Tat system activity and iron assimilation suggesting a modality by which this lipoprotein is involved in *Y. pestis* pathogenesis.

Author summary

We have previously shown that the NlpD lipoprotein, which is involved in the regulation of cell morphogenesis, is essential for virulence of the plague bacteria, *Yersinia pestis*. To uncover the role of NlpD in *Y. pestis* pathogenicity, we conducted a whole-genome comparative transcriptome analysis as well as phenotypic and virulence evaluation analyses of the *nlpD* and related mutants. The study reveals a new role for the *Y. pestis* NlpD lipoprotein in iron assimilation and Tat system activity.

Introduction

Bacteria and in particular bacterial pathogens have successfully evolved sophisticated mechanisms that allow them to sense, cope and adapt to varying conditions in their immediate surroundings. The rapid detection of extracellular signals such as the concentrations of nutrients, ion sources, temperature, stress conditions and the presence of host immune cells, influence transcriptional regulatory systems that in turn lead to physiological and morphological changes that enable the organism to survive within hostile environments such as those encountered in the host during infection [1].

The Gram-negative pathogen *Yersinia pestis* is the causative agent of plague, a disease that has inflicted millions of deaths in three world pandemics [2]. Plague still persists in Africa, Asia and the Americas and as of today, it is categorized as a re-emerging disease [3]. The prevalent form of the disease is bubonic plague, which develops following transmission of the pathogen from rodent reservoirs to humans via infected fleas and has high mortality rate if untreated [4,5]. Primary pneumonic plague, which represents one of the most severe forms of the disease, is less abundant in nature and results from the inhalation of *Y. pestis*-containing droplets or aerosols. Pneumonic plague is a contagious rapidly progressing disease that leads to 100% mortality in untreated patients [2]. These characteristics as well as the inhalational nature of infection led to the recognition of plague as a bioterror threat agent [6].

The ability of *Y. pestis* to invade the mammalian host, colonize internal organs and overcome the immune response is attributed to the combined activities of multiple virulence pathways that are activated in a timely manner during infection in response to the host *milieu* signals [7,8]. Some of these pathways have been demonstrated to be absolutely required for the bacterial pathogenesis in animal models. These include molecular systems that enable the acquisition of essential nutrients during infection as well as those required for evading the host immune response such as the type 3 secretion system (T3SS) [9,10,11,12,13,14,15,16,17,18,19].

We have previously documented that the NlpD lipoprotein is essential for *Y. pestis* virulence in animal models of plague infection and that the *nlpD* mutant is impaired in its ability to colonize internal organs [20]. NlpD is conserved among Gram-negative bacteria and exhibits characteristic LysM and LytM domains found in enzymes involved in bacterial cell wall remodeling [21,22]. Consistent with this known biological role of LytM-containing proteins, the phenotype of the *Y. pestis nlpD*-disrupted mutant is characterized by altered chain-forming cell morphology [20]. Interestingly, despite its substantial virulence attenuation, the mutant was not affected in terms of *in vitro* growth or in the activity of the T3SS [20], which is essential for the pathogenicity of the bacteria. To gain further insights into the role of NlpD in the manifestation of *Y. pestis* virulence, we extended the characterization of the *nlpD* mutant in the present study by performing transcriptomic, phenotypic, and molecular genetic analyses. Integration of the results led to the unexpected finding that in *Y. pestis*, NlpD is required for iron assimilation and for the activity of the twin-arginine system (Tat) which translocates folded proteins across the bacterial cytoplasmic membrane in a wide range of bacteria [23]. Systematic deletion mutagenesis of Tat genes in the virulent *Y. pestis* Kim53 strain indicated that the Tat system is required for *Y. pestis* iron assimilation as well as virulence manifestation in the mouse plague infection models.

Materials and methods

Ethics statement

This study was carried out in strict accordance with the recommendation in the Guide for the Care and Use of Laboratory Animals of the National Institute of Health. All animals

experiments were performed in accordance with Israeli law and were approved by the Ethics Committee for animal experiments at the Israel Institute for Biological Research (Protocols M-03-16, M-81-16, M-57-11).

Bacterial strains, plasmids and mutant construction

The *Y. pestis* strains and plasmids used in this study are listed in Table 1. Construction of the Kim53 deletion mutants was performed by replacing part of the gene coding sequence with a linear fragment containing a resistance cassette by homologous recombination using previously established methodologies [16]. The sequence that was deleted from the *Y. pestis* genome in each mutant is indicated in Table 1.

Deletion of the *Y. pestis nlpD* gene has been described previously [20]. Deletion of the *Y. pestis tata*, *tatB* and *tatC* and *amiC* genes was performed using a linear fragment containing a kanamycin resistance gene that was amplified from pKD4 plasmid and used for homologous recombination as described in [27]. Deletion of the *tata*, *tatB*, *tatC* and *amiC* genes from the *Y. pestis* genome was verified by PCR analysis. TatC expression was monitored by Western

Table 1. *Y. pestis* strains and plasmids used in this study.

<i>Y. pestis</i> strains and plasmid	Relevant characteristic(s)	Reference or source
Strains		
Kimberley53 (Kim53)	Virulent strain	[24]
EV76	Vaccine strain, Δ <i>pgm</i> strain	[15]
Kim53 Δ <i>nlpD</i>	Kim53 strain in which bp 112 to 318 (out of 999) of the <i>nlpD</i> gene were deleted; kan ^R	[20]
Kim53 Δ <i>tata</i>	Kim53 strain in which bp 10 to 255 (out of 267) of the <i>tata</i> gene were deleted; kan ^R	This study
Kim53 Δ <i>tatB</i>	Kim53 strain in which bp 13 to 645 (out of 663) of the <i>tatB</i> gene were deleted; kan ^R	This study
Kim53 Δ <i>tatC</i>	Kim53 strain in which bp 18 to 771 (out of 774) of the <i>tatC</i> gene were deleted; kan ^R	This study
Kim53 Δ <i>amiC</i>	Kim53 strain in which bp 57 to 1198 (out of 1251) of the <i>amiC</i> gene were deleted; kan ^R	This study
Kim53 Δ <i>nlpD</i> + <i>pnlpD</i>	Kim53 Δ <i>nlpD</i> + <i>pnlpD</i> complemented strain	[20]
Kim53pTorA _{signal} -GFP	Kim53 + pTorA _{signal} -GFP plasmid	This study
Kim53 Δ <i>nlpD</i> pTorA _{signal} -GFP	Kim53 Δ <i>nlpD</i> + pTorA _{signal} -GFP plasmid	This study
Kim53 Δ <i>tata</i> pTorA _{signal} -GFP	Kim53 Δ <i>tata</i> + pTorA _{signal} -GFP plasmid	This study
Kim53 Δ <i>tatB</i> pTorA _{signal} -GFP	Kim53 Δ <i>tatB</i> + pTorA _{signal} -GFP plasmid	This study
Kim53 Δ <i>tatC</i> pTorA _{signal} -GFP	Kim53 Δ <i>tatC</i> + pTorA _{signal} -GFP plasmid	This study
Kim53 Δ <i>tata</i> <i>ptatA</i>	Kim53 Δ <i>tata</i> + <i>ptatA</i> plasmid	This study
Kim53 Δ <i>tatC</i> <i>ptatC</i>	Kim53 Δ <i>tatC</i> + <i>ptatC</i> plasmid	This study
Kim53p: <i>gadC</i> :GFP	Kim53+ (pCA24N: <i>gadC</i> +GFP) plasmid	This study
Kim53p: <i>btuC</i> :GFP	Kim53+ (pCA24N: <i>btuC</i> +GFP) plasmid	This study
Kim53p: <i>napG</i> :GFP	Kim53+ (pCA24N: <i>napG</i> +GFP) plasmid	This study
Kim53 Δ <i>nlpD</i> : <i>gadC</i> :GFP	Kim53 Δ <i>nlpD</i> + (pCA24N: <i>gadC</i> +GFP) plasmid	This study
Kim53 Δ <i>nlpD</i> : <i>btuC</i> :GFP	Kim53 Δ <i>nlpD</i> + (pCA24N: <i>btuC</i> +GFP) plasmid	This study
Kim53 Δ <i>nlpD</i> : <i>napG</i> :GFP	Kim53 Δ <i>nlpD</i> + (pCA24N: <i>napG</i> +GFP) plasmid	This study
Kim53 Δ <i>nlpD</i> + <i>pnlpD</i> : <i>napG</i> :GFP	Kim53 Δ <i>nlpD</i> + <i>pnlpD</i> complemented strain [20] + (pCA24N: <i>napG</i> +GFP) plasmid	This study
Plasmids		
<i>ptatA</i>	The complete <i>tata</i> coding sequence inserted into the pWKS30 plasmid (HindIII, XbaI), lac promoter; ampR	This study
<i>ptatC</i>	The complete <i>tatC</i> coding sequence inserted into the pWKS30 plasmid (HindIII, XbaI), lac promoter; ampR	This study
pTorA _{signal} -GFP	pBR322 with TorA signal fused to GFPuv protein	[25]
pCA24N- <i>gadC</i>	Plasmid from ASKA collection (pCA24N) + <i>gadC</i> gene fused to GFP	[26]
pCA24N- <i>btuC</i>	Plasmid from ASKA collection (pCA24N) + <i>btuC</i> gene fused to GFP	[26]
pCA24N- <i>napG</i>	Plasmid from ASKA collection (pCA24N) + <i>napG</i> gene fused to GFP	[26]

<https://doi.org/10.1371/journal.pntd.0007449.t001>

blot analysis in the *tatA* and *tatB* mutants to test for possible polar effect on TatC expression (S1 Fig). The analysis indicated that *tatC* expression was not affected by the *tatA* mutation yet it was affected in the *tatB* mutant, and therefore the *tatB* mutant was excluded from the analysis documented in this report (S1 Fig).

The pTorA_{signal}-GFP [25] and pCA24N-*napG* [26] plasmids were used to test the functionality of the Tat system in *Y. pestis*.

For complementation of the *tatA* and *tatC* deletion mutants, each of the respective *tat* genes was cloned into the low copy plasmid pWKS30 [28]. Primers pWKS-*tatA*-For and pWKS-*tatA*-Rev for the *tatA* gene and primers pWKS-*tatC*-For and pWKS-*tatC*-Rev for *tatC* gene were used for PCR amplification from *Y. pestis* Kim53 DNA (S1 Table). The PCR products were digested with XbaI and HindIII, and then cloned into the pWKS30 vector to generate the pWKS-*tatA* and pWKS-*tatC* amp^r plasmids. The plasmids were transformed into the compatible *Y. pestis* deletion mutant. PCR analysis verified that all the newly constructed mutants carried the pMT1, pCD1 and pPCP1 plasmids and the chromosomal *pgm* locus.

Bacterial growth conditions

Y. pestis strains were routinely grown on brain heart infusion agar (BHIA, BD, MD USA) for 48 h at 28°C. The *nlpD* and *tat* mutants were grown on BHIA supplemented with 50 µg/ml kanamycin (Sigma-Aldrich, Israel), and all complemented *Y. pestis* mutant were grown on BHIA supplemented with 100 µg/ml ampicillin.

For bacterial total RNA preparation, bacterial colonies were grown on BHIA plates for 48 h at 28°C, harvested and diluted in heart infusion broth (HIB) (BD, USA) supplemented with 0.2% xylose and 2.5 mM CaCl₂ (Sigma-Aldrich, Israel) to an OD₆₆₀ of 0.01 and grown overnight (o.n.) at 28°C in a shaker (200 rpm). The resulting cultures were diluted in fresh broth to an OD₆₆₀ of 0.05 and allowed to grow for 5 h at 37°C. Aliquots of ~5×10⁸ colony forming units (cfu) were collected by centrifugation and the cells were immediately frozen in liquid nitrogen and stored at -70°C until use.

To assess growth under iron limiting conditions, we followed protocols established at the Perry and Fetherston laboratory [29]. Several isolated colonies grown for 48 h at 28°C on a BHIA plate were collected for o.n. growth at 28°C in PMH2 medium [30] [31]. The next day, 0.1 OD₆₆₀ of the o.n. cultures was inoculate into fresh PMH2 grown for 6–7 h at 37°C and then diluted to 0.1 OD₆₆₀ with fresh PMH2 and grown o.n. at 37°C. The next morning, the cultures were diluted again to 0.1 OD₆₆₀ with PMH2 and 10µl drops containing ~10⁶ bacilli were plated on iron-depleted, gradient plates and incubated for ~50 h at 37°C. Gradient plates were prepared using square plates (USA scientific, 5668–8102) to which was added a total of 70 ml of medium was added, 35 ml for the bottom layer (poured on a slope) and 35 ml for the top layer, which was poured 24 h before performing the growth assay. The bottom layer contained 1% agarose, 1× PMH2, 20 µM MgCl₂ and 100 µM 2,2'-dipyridyl (DIP) as a chelator. The top layer contains 1% agarose, 1× PMH2 and 20 uM MgCl₂ (no chelator). In this manner, a DIP gradient was established ranging between 0 and 100 mM. In addition, plates containing 1% agarose, 1× PMH2, 20 µM MgCl₂ and 80 or 100 µM DIP were prepared [32] and 10µl drops containing ~10⁶ bacilli were plated and incubated for ~50 h at 37°C as described above. To rescue bacterial growth on plates containing 100 µM DIP, iron dextran (d8517, Sigma-Aldrich) was added to the medium at a concentration of 0.5 mg/ml.

To evaluate the functionality of the Tat system, bacteria containing pTorA_{signal}-GFP or pCA24N constructs (Table 1) were grown o.n. at 28°C in HIB supplemented with 0.2% xylose and 2.5 mM CaCl₂ (Sigma-Aldrich, Israel) containing 100 mg/ml ampicillin, and the next-day cultures were diluted to OD₆₆₀ of 0.05 into 15 ml culture and grown at 37°C. After incubation

for 5–7 h, 5 ml of each culture was centrifuged (10,000 g), and the cell pellets were washed with 5 ml of double-distilled water (DDW). The cells were centrifuged and then resuspended to an OD₆₆₀ of 0.01 with DDW. For morphological analysis, bacterial cells were washed with DDW twice and diluted to an OD₆₆₀ of 0.01.

RNA isolation, labeling, hybridization and microarray analysis

Total RNA was purified using the RNeasy-Mini Kit (QIAGEN) according to the manufacturer's instructions. Seven micrograms of total RNA was used for microarray analysis of each sample using the FairPlay III microarray labeling kit (Stratagene) according to the manufacturer's instructions. To examine changes in expression of *Y. pestis* genes, a custom array was used [33]. The array contains 4196 coding regions and pseudogenes out of the 4321 predicted genes of the *Y. pestis* CO92 strain (Acc no.: NC_003143, NCBI). Hybridization and scanning were performed as suggested by Agilent. The slides were scanned in an Agilent DNA Microarray Scanner G2505B. Images were analyzed and data were extracted using Agilent Feature Extraction software version 9.5.1.1 (FE), with linear and lowess normalization performed for each array. A reference design with two biological replicates was applied to compare the wild-type Kim53 strain and the $\Delta nlpD$ mutant. Statistical analysis was performed using the Limma (Linear Models for Microarray Data) package from the Bioconductor project (<http://www.bioconductor.org>). The processed signal resulting from the FE was read into Limma using the "read.maimages" function. Background subtraction and lowess normalization were performed within each array. A quantile normalization between arrays was applied. Standard quality control was performed using the plot functions of Limma [34]. Differential expression was assessed using linear models for designed microarray experiments. The fold changes (FC) and standard errors were estimated by fitting a linear model for each gene and applying empirical Bayes smoothing to the standard errors [34]. The FDR (false discovery rate) was controlled using the method of Benjamini and Hochberg for multiple comparisons [35,36].

The P value is the result of a one-sample Student's t test, which was applied to the natural log of the mean of each normalized value against the baseline value of 0. Genes with differences corresponding to $P < 0.05$ in either the high or the low photomultiplier scans and that had signal-to-control or control-to-signal ratios ≥ 2.0 were considered to be differentially regulated. The results were submitted to the GEO depository and are available online (<http://www.ncbi.nlm.nih.gov/geo/>, record GSE101490).

Quantitative real-time PCR (qRT-PCR)

For qRT-PCR analysis, 2 μ g of total RNA was reverse-transcribed using the Reverse Transcription (RT) System kit (Promega) with random primers according to the manufacturer's instructions. The cDNA was used as a template for qRT-PCR with specific primers (S1 Table) using an ABI 7500 instrument (Applied Biosystems, USA) with SYBR green PCR master mix (Applied Biosystems, USA). Relative quantification was determined using an average of 2 genes: YPO1045 (*tsf* gene) and YPO1415 (*pyrD* gene), for standardization of all qRT-PCR results using the comparative ($-2^{\Delta\Delta Ct}$) method. Forty cycles of PCR amplification were performed in duplicate for each primer set.

Western blot analysis

For Western blot analysis, bacterial colonies were grown on BHIA plates for 48 h at 28°C, harvested and diluted in heart infusion broth (HIB) (BD, USA) supplemented with 0.2% xylose and 2.5 mM CaCl₂ (Sigma-Aldrich, Israel) to an OD₆₆₀ of 0.05 and grown at 37°C in a shaker (200 rpm). Bacteria (OD₆₆₀ = 0.1) were lysed in Laemmli Sample buffer (Bio-Rad) and protein

concentrations were determined using bicinchoninic acid (BCA Protein Assay Reagent, Pierce) according to the manufacturer's instructions. Equal amounts of protein were loaded and separated by SDS-PAGE. After transfer to nitrocellulose membranes, duplicate membranes were developed with anti-peptide antibodies against NlpD, Pcm [20] and TatC (see below). Probing with the primary antibody was followed by incubation of the membranes with HRP-conjugated secondary antibody (A6154, Sigma-Aldrich) visualized using the LAS-3000 imaging system (Fuji) or by IRDye 680RD-conjugated secondary antibodies (LIC-92668071 and LIC-92668070 LI-COR) visualized using the Odyssey CLx imaging system from LI-COR. The TatC anti-peptide antibodies were raised by immunizing rabbits with maleimide-activated KLH (Pierce) conjugated to the synthetic peptides CYNLVSAPLIKQLPAGAS (amino acids 41–59 out of 258aa of TatC).

Microscopy of bacterial cultures

For the morphological analysis, 5µl bacterial aliquots were placed in an 8-well slide (#5638–01940, Bellco Glass) to dry. Cells were fixed with cold methanol (–20°C) for 15 minutes and Gram stained according to the manufacturer's instructions (HT90A kit, Sigma-Aldrich). Images were captured under a Nikon Eclipse E200 microscope connected to a Nikon DS-Fi-1 camera at a magnification of ×400 and ×1000.

For the Tat and Sec functionality analysis, bacterial cells were mounted on poly L-lysine-treated microscope slides with Fluoromount-G (Southern Biotechnology, Birmingham, AL) and covered with a glass coverslip. The slides were examined by phase-contrast and fluorescence (fluorescein isothiocyanate filter set) microscopy. The images shown were analyzed using Zeiss LSM 710 Confocal Microscope (Zeiss, Oberkochen, Germany). Fluorescence intensity quantification of the above-mentioned markers was performed using Zen1 software, Zeiss.

For DAPI and TatC labeling of bacterial cells, approximately 10^6 cfu were placed in a well on a DoubleCytoslide (Thermo). The cells were dried for 30 minutes and fixed with cold methanol (–20°C) for 10 minutes. The slides were then transferred to 80% cold acetone (–20°C) for 30 seconds and allowed to dry. Blocking was performed for 15 minutes with 2% BSA (in PBS). Slides were washed with DDW 3 times and then labeled with a primary αTatC antibody for 1 hour (2% BSA, 0.05% Tween 20 suspended in PBS), washed 5 times with PBS and then labeled for 15 minutes with a secondary anti-rabbit antibody labeled with Alexa 594 succinimidyl ester.

Labeling of *Y. pestis* cells was performed with αF1 antibodies generated against the F1 capsular protein [37] and linked to FITC or with antibodies generated against the bacterium [38] and linked to Alexa fluor 647. After labeling, the slides were washed 5 times in DDW, labeled by DAPI staining for 2 minutes, washed two times with DDW, covered and mounted with cover glasses and allowed to dry in the dark. For fluorescence microscopy, the cells were captured using a Zeiss LSM 710 confocal microscope (Zeiss, Oberkochen, Germany).

TorA signal-GFP export assay

The assay was performed according to Alcock *et al.*, [39]. Briefly, overnight HIB culture of *Y. pestis* strains bearing the pTorA_{signal}-GFP plasmid were grown at 28°C. Cultures were diluted the next morning to 0.1 OD₆₆₀ and grown for 6 hours at 37°C. Cells were harvested and washed twice in 10 mM Tris.Cl, 150 mM NaCl, pH 7.3.

Equal volumes of the cell suspensions (10 OD₆₆₀) were then centrifuged, and the cell pellets resuspended in 1ml SET buffer (17.12% sucrose (w/v), 3 mM EDTA, 10 mM Tris.Cl, pH 7.3), and left at room temperature for 20 min. Cell were concentrated in the 2 ml Eppendorf tubes

at maximum speed for 10 min (20,000x g). The cell pellet was resuspended in 250 μ l lysozyme (3 mg/ml in water) and 750 μ l ice-cold water and incubated for 20 min at 37°C. Spheroplasts were released from the periplasm by centrifugation at maximum speed for 10 min (20,000x g). Samples were analyzed by immunoblotting for GFP (α GFP antibodies, G1546, sigma-aldrich, Israel) or the cytoplasmic marker protein Pcm [20]. The data presented is representative of at least two independent experiments.

Sec translocon assay

Assessment of Sec functionality in *Y. pestis* strains was performed following transformation with two plasmids from the ASKA collection [26] encoding the Sec substrates BtuC and GadC fused to GFP. These plasmids were a kind gift from professor Eitan Bibi [40]. *Y. pestis* wild-type and $\Delta nlpD$ strains were grown on BHI agar plates with chloramphenicol (25 mg/ml) for 48 h. The cells were resuspended to a final concentration of 0.2 OD₆₆₀/ml in PBS. Fluorescence of the $\Delta nlpD$ was quantified using a Victor3 (PerkinElmer) instrument with wavelength of 485nm (excitation) and 535nm (emission) and presented relatively to the wild type strain [40].

Animal studies

Female CD1 mice (5–6 weeks old) were purchased from Charles River (UK) and maintained under defined flora conditions at the animal facilities of the Israel Institute for Biological Research. The subcutaneous infections were performed as described previously [41]. Briefly, bacterial colonies grown on BHIA plates for 48 h at 28°C were harvested and suspended in saline solution to the required infection dose and quantified by counting cfu after plating and incubating on BHIA plates (48 h at 28°C). The intranasal (i.n.) infections were performed as described previously [20]. Briefly, bacterial colonies were grown in HIB supplemented with 0.2% (+) xylose and 2.5 mM CaCl₂ and incubated overnight at 28°C. Cultures were diluted in saline solution to the required infection dose and quantified by cfu counting. Prior to infection, mice were anaesthetized with a mixture of 0.5% ketamine HCl and 0.1% xylazine was injected intraperitoneally followed by i.n infection with 35 μ l/mouse of the bacterial suspension. The LD₅₀ experiments were performed using groups of five mice. The LD₅₀ values were calculated according to the method described by Reed and Muench [42],[15].

To evaluate the complementation of virulence by iron supplementation, mice (n = 6) received 5 mg iron-dextran (d8517, Sigma-Aldrich) intraperitoneally (i.p) 2 to 3 h before s.c. inoculation of 1×10^7 cfu of the *Y. pestis* strains. Beginning on the second day post-infection, iron dextran (5 mg/mouse) was administered once daily i.p. during the course of the experiment.

Statistical analysis

Statistical significance was measured using the Student's unpaired t test. Survival curves were compared using the log-rank test. In all analyses, *p* values equal to 0.05 served as the limit of significance. Calculations were performed using GraphPad Prism 5 statistical pack.

Results

Transcriptomic analysis and functional classification of the differentially expressed genes in wild-type and $\Delta nlpD$ *Y. pestis* strains

To elucidate pathways by which NlpD is required during plague infection, we compared the transcriptional profiles of the parental virulent *Y. pestis* Kim53 strain and its isogenic *nlpD*

mutant grown under conditions reminiscent of early stages of infection of the mammalian host.

Total RNA was prepared from *Y. pestis* cultures grown at 28°C, transferred to 37°C for five hours and then used as template for cDNA synthesis. Fluorescently labeled cDNA served as a probe for hybridization to a custom *Y. pestis* array [33]. A total of 220 genes were differentially expressed in the *nlpD* mutant (≥ 2 -fold change in two experimental repeats, $P < 0.05$) compared with the *Y. pestis* Kim53 strain. Among these genes, 113 were up-regulated (S2 and S4 Tables, S2A Fig) and 107 were down-regulated (S3 and S5 Tables, S2B Fig) in the mutant strain. The microarray data were validated by qRT-PCR analysis of the mRNA levels of selected genes. Plotting the data obtained using two complementary approaches revealed a strong positive correlation, confirming the microarray results ($R^2 = 0.846$, see Supplementary S3 Fig, S6 Table).

Inspection of the functional annotation of the 220 differentially expressed genes (inferred from the NCBI and KEGG databases (<https://www.ncbi.nlm.nih.gov/gene/> and <http://www.genome.jp/kegg>, respectively) indicated that membrane stress response was induced in the *nlpD* mutant (S2 Table) and iron-related metabolic pathways as well as transport systems for nutrients such as sulfate, arginine and sugar were differentially regulated (S2 Table and S3 Table). Two of the genes that were most significantly up-regulated in the mutant strain were *cpxP* and *pspA* (15.82-fold and 3.5-fold, respectively, S2 Table), belonging to the membrane stress response pathways Cpx (conjugative plasmid expression) and Psp (phage shock protein). These two pathways are involved in maintaining the homeostasis of the cytoplasmic membrane and preventing damage resulting from the accumulation of misfolded proteins in the periplasm [43,44]. These results suggest that in the absence of the NlpD lipoprotein, misfolded protein accumulation is increased in the periplasm. Activation of the Cpx and Psp stress response pathways may therefore represent a compensatory modality for retaining the integrity of the *nlpD* mutant membranes.

As indicated, many of the differentially modulated genes in the *nlpD* mutant were related to iron metabolism (~ 20%). Iron is an essential nutrient for most pathogenic bacteria and for *Y. pestis* in particular [45,46]. Some iron uptake systems involve an outer membrane receptor, a periplasmic binding protein and an inner membrane ATP-binding cassette (ABC) transporter. Coupling of the proton motive force of the cytoplasmic membrane to the outer membrane by the TonB, ExbB, and ExbD proteins provides the energy required for transport. Interestingly, genes that are up-regulated in the *nlpD* mutant (S2 Table) included the *exbBD-tonB* genes as well as the *ybtA* transcriptional regulator of the major iron acquisition system Yersiniabactin (Ybt) and the *irp5* gene of this system required for synthesis of the Yersiniabactin siderophore [47]. Genes encoding additional iron uptake and storage systems such as Yiu, Fit and the ferri-chrome and ferrisiderophore receptor proteins were also up regulated in the *nlpD* mutant. These results, which indicate a compensatory up-regulation of iron uptake systems, strongly suggest that the *nlpD* mutant has a limited ability to acquire iron from the environment. Inspection of the down-regulated genes in the *nlpD* mutant suggest that in response to the apparent shortage of iron, deletion of the *nlpD* gene results in the decreased expression of several iron-containing proteins (fumarate reductase, dimethyl sulfoxide reductase and nitrate reductase) as well as the expression of the IscR transcription factor, which has been shown to modulate the expression of iron-sulfur protein clusters in *Escherichia coli* [48]. Similarly, the expression of proteins that are active in metabolic processes involving Fe-S-containing proteins was down regulated probably to preserve the small amount of intracellular iron for more essential metabolic pathways (S3 Table). The suggested paucity of iron in the *nlpD* mutant is also supported by the observed decreased expression of the *ccmA-ccmH* gene cluster (S3 Table) encoding a heme export system that functions in *E. coli* in cytochrome c maturation

[49]. Iron is required for the activity of many enzymes of the tricarboxylic acid cycle, the cytochromes, non-heme iron electron carriers of the electron transport chain and nitrogen assimilation [50]. Indeed, metabolic pathways that utilize enzymes that are co-factored by iron were down-regulated in the *nlpD* mutant, leading to a metabolic shift in comparison to the wild-type strain (S3 Table). Taken together, these results strongly suggest that the *nlpD* mutant has a limited ability to acquire iron from the environment, a characteristic which could not have been anticipated solely from the documented function of NlpD in cell wall remodeling.

***Y. pestis* NlpD lipoprotein is required for growth under iron-limiting conditions**

To confirm the hypothesis drawn from the transcriptomic analysis that the *nlpD* mutant has limited iron assimilation, the *nlpD* mutant and the parental Kim53 strains were analyzed using an *in vitro* growth assay under iron-limiting conditions [29]. Indeed, growth of the *nlpD* mutant was impaired in comparison to the wild-type strain under the iron-deficient conditions induced by addition of the iron-chelating agent 2,2'-dipyridyl (DIP) to the PMH2 defined medium (Fig 1A). Consequently, the limitation of the *nlpD* mutant to acquire iron during growth could also be manifested *in vivo* during infection and therefore may represent the cause for its avirulent phenotype in the mouse model of plague. To directly address this possibility, reversion of the avirulent phenotype of the *nlpD* mutant was attempted by exogenous administration of iron to the *Y. pestis nlpD*-infected mice. Such an approach has been previously described for studying the phenotype of an EV76 attenuated *Y. pestis* strain lacking the Ybt iron acquisition system carried in the *pgm* genomic region [51]. Thus, mice were subcutaneously infected with a single dose of 1×10^7 cfu of EV76 or with a similar dose of the attenuated *nlpD* mutant. As shown in Fig 1B, the virulence of the EV76 strain, but not of the *nlpD* mutant, was restored by daily injection of iron dextran.

***Y. pestis* NlpD lipoprotein is required for functionality of the twin-arginine translocation system**

A possible explanation for the inability to revert the attenuated phenotype of the *nlpD* mutant by exogenous addition of iron is the existence of additional defects that prevent establishment of infection by the *nlpD* mutant. Apart from attenuation of virulence, the *Y. pestis nlpD* phenotype has thus far been characterized to include, impaired cell septation, slight sensitivity to acidic stress conditions, and the above deficiency in iron acquisition (Fig 1A) [20]. This set of phenotypes was reminiscent of the phenotypes characterizing the twin-arginine translocation system (Tat) mutants of Gram-negative bacteria [52]. The Tat system typically consists of three cytoplasmic membrane proteins: TatA, TatB, and TatC, which are encoded by a single operon and are responsible for the transport of folded proteins across the cytoplasmic membrane [53,54]. Proteins that are translocated by the Tat system include cofactor-containing enzymes, multimeric proteins that require assembly prior to export as well as integral membrane proteins [53,55,56,57]. Tat substrates function in energy metabolism, cellular division, motility and adaptation to environmental stress [52,58]. The system has been shown to be important for virulence in many bacterial pathogens including *Yersinia* species [25,52,59,60,61].

To examine the functionality of the Tat system in the *nlpD* mutant, an established method based on the GFP reporter protein fused to the TorA Tat signal was used [62]. In the wild type *Y. pestis* background, GFP was localized to the periplasm and enriched at the cell poles whereas in *Y. pestis* TatA and TatC mutants, localization to the periplasm and poles was lost and the GFP reporter protein was diffused completely throughout the cytoplasm (Fig 2A). This

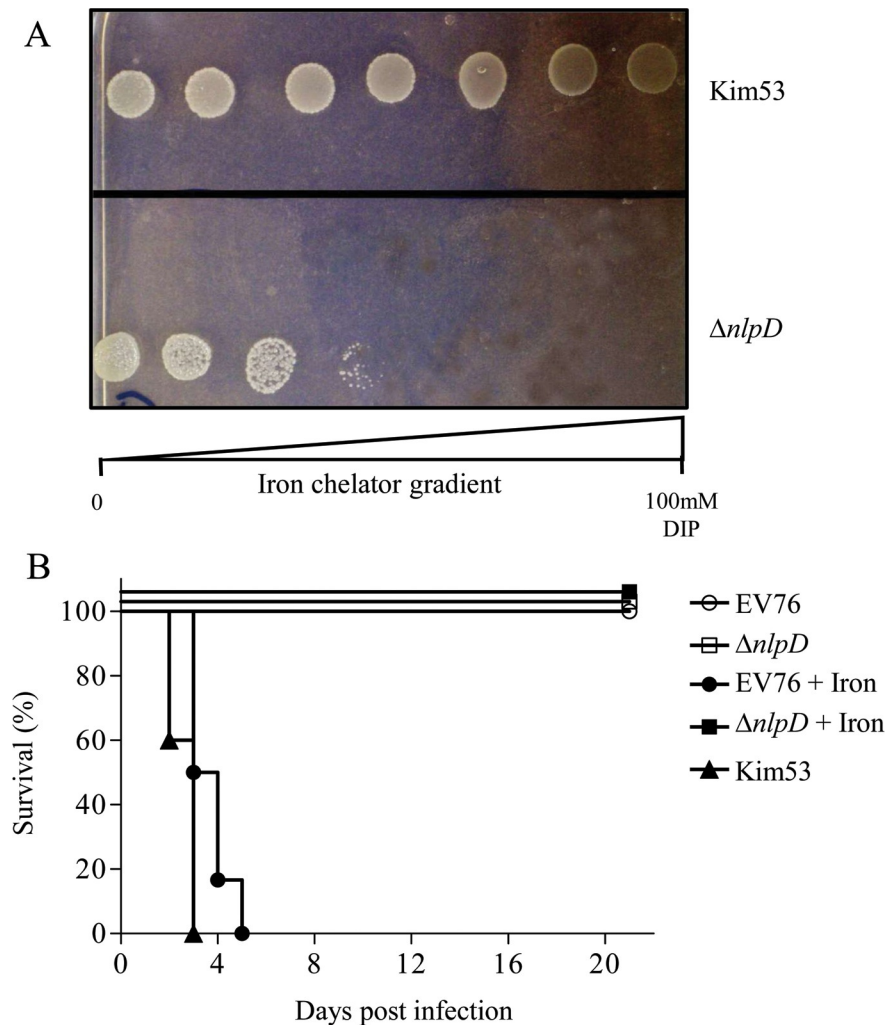


Fig 1. Role of iron in *nlpD* mutant growth and pathogenesis. A. Growth of *Y. pestis* strains under iron-limiting conditions. Kim53 (upper panel), Kim53 $\Delta nlpD$ (lower panel). The displayed data is one representative experiment. B. Survival curves of iron-treated mice infected with attenuated *Y. pestis* strains. Two groups of 12 mice were infected with the attenuated *Y. pestis* EV76 (circles) or Kim53 $\Delta nlpD$ (square) strains (s.c. infection with 10^7 cfu/mouse). In each group, six mice were treated with iron dextran (filled symbols), and six mice served as control (open symbols). Survival curve of mice infected with the *Y. pestis* Kim53 strain (s.c. infection with 10^6 cfu/mouse, triangles).

<https://doi.org/10.1371/journal.pntd.0007449.g001>

observation is consistent with previous observations for other bacterial pathogens [25,60]. In the *nlpD* mutant, the GFP reporter was completely diffused throughout the cytoplasm, as observed for the Tat mutants, suggesting loss of Tat activity (Fig 2A). Of note, mutation of the *tatB* gene resulted in a polar phenotype abrogating expression of both TatB and TatC subunits (see Materials and Methods), therefore the *tatB* mutant was excluded from the current analysis. To further confirm the loss of Tat functionality in the *nlpD* mutant strain, the cellular localization of NapG, an additional Tat-substrate protein was investigated [60]. Accordingly, a hybrid protein consisting of the full length NapG protein and a C-terminal fused GFP reporter [26], was expressed in the parental wild-type, $\Delta nlpD$ mutant, as well as in the NlpD trans-complemented strain. The data (S4 Fig) clearly establish that the *nlpD* mutation is accompanied by the loss of fluorescence polarity that is characteristic for the Tat dysfunctionality. Furthermore this disturbed localization was fully alleviated upon trans-complementation of the *nlpD*

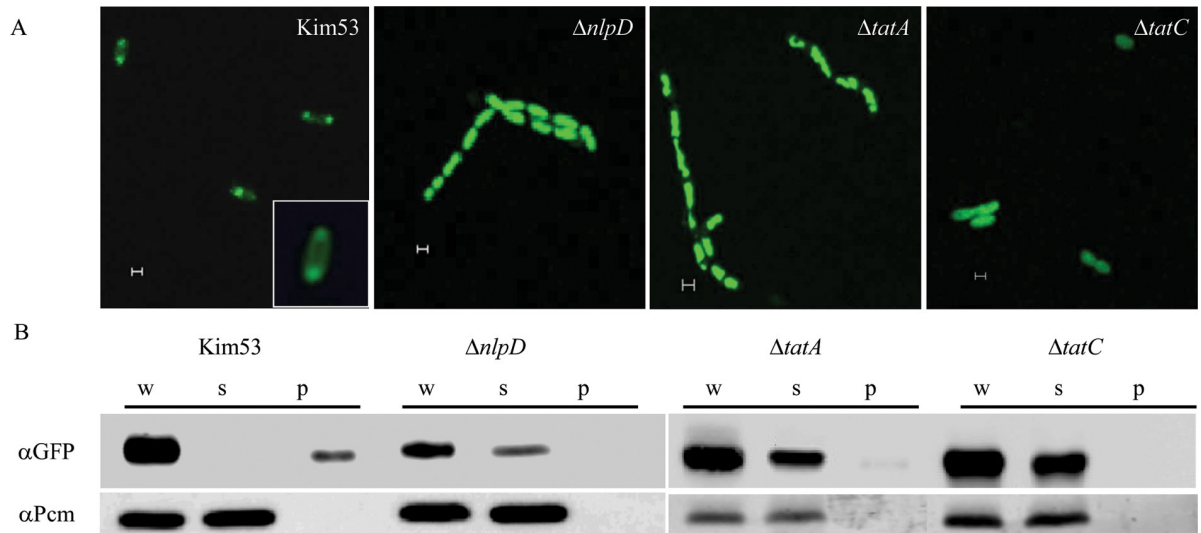


Fig 2. Intracellular localization of the TorA_{signal}-GFP Tat-reporter protein in *Y. pestis* strains. A. *Y. pestis* strains Kim53:pTorA_{signal}-GFP, Kim53 $\Delta nlpD$:pTorA_{signal}-GFP, Kim53 $\Delta tatA$:pTorA_{signal}-GFP, and Kim53 $\Delta tatC$:pTorA_{signal}-GFP, were inspected under a fluorescence microscope for identification of TorA_{signal}-GFP localization. The scale bar represents 1 μ m. B. *Y. pestis* cells overproducing TorA_{signal}-GFP were fractionated into Whole cell (W), spheroplast (S) and periplasm (P), and were subject to immunoblotting with antibodies against GFP or against the cytoplasmic protein Pcm [20]. The blots were derived from the same experiment and were processed in parallel. The data presented are representative of at least two independent experiments and the displayed data is one representative experiment.

<https://doi.org/10.1371/journal.pntd.0007449.g002>

mutant with an NlpD-expressing construct (S4 Fig) that was also shown to restore the wild-type cell morphology and virulence phenotype [20].

The direct assessment of Tat-substrate localization in *nlpD* mutant cells by microscopy described above was further substantiated by inspection of subcellular localization of a Tat substrate reporter in Tat mutant strains which were engineered by specifically disrupting expression of each of the Tat subunits (see Table 1). Thus, the functionality of the Tat system was interrogated implementing the molecular approach [39,63] consisting of Western blot analysis of fractionated material obtained from the various mutants as well as the parental strain. The Western-blot analysis of the subcellular fractions of the *Y. pestis* strains clearly confirmed that Tat transport was substantially affected in the *nlpD* mutant as seen for the *tatA* and *tatC* mutants (Fig 2B, S5 Fig). These results indicated, as anticipated, that the Tat system is not functional in the *nlpD* mutant and that the *Y. pestis* NlpD lipoprotein is required, directly or indirectly, for Tat system functionality.

Interestingly, the mRNA levels of all Tat genes (TatA, TatB and TatC) quantified in the *nlpD* mutant were indistinguishable to those of the wild-type strain, according to the microarray transcriptome analysis (<http://www.ncbi.nlm.nih.gov/geo/>, record GSE101490) and unambiguously confirmed by the qRT-PCR quantification of *tatC* mRNA (Fig 3A). However, Western blot analysis of TatC protein (used as a representative component for the Tat system) indicated that the protein level was reduced in the *nlpD* mutant in comparison to the wild-type strain (Fig 3B, S6 Fig). A dramatic difference between the wild type strain and the *nlpD* mutant was also observed in the confocal microscopy images of bacterial cells labeled with anti-TatC antibodies (Fig 3C). In these images, regions of fluorescence identified by anti-TatC antibodies were clearly visible throughout the cytoplasmic membrane of DAPI-stained wild-type *Y. pestis* bacteria (Fig 3C, upper panel), whereas no signal could be detected in DAPI-stained cells of the *nlpD* mutant (Fig 3C, lower panel).

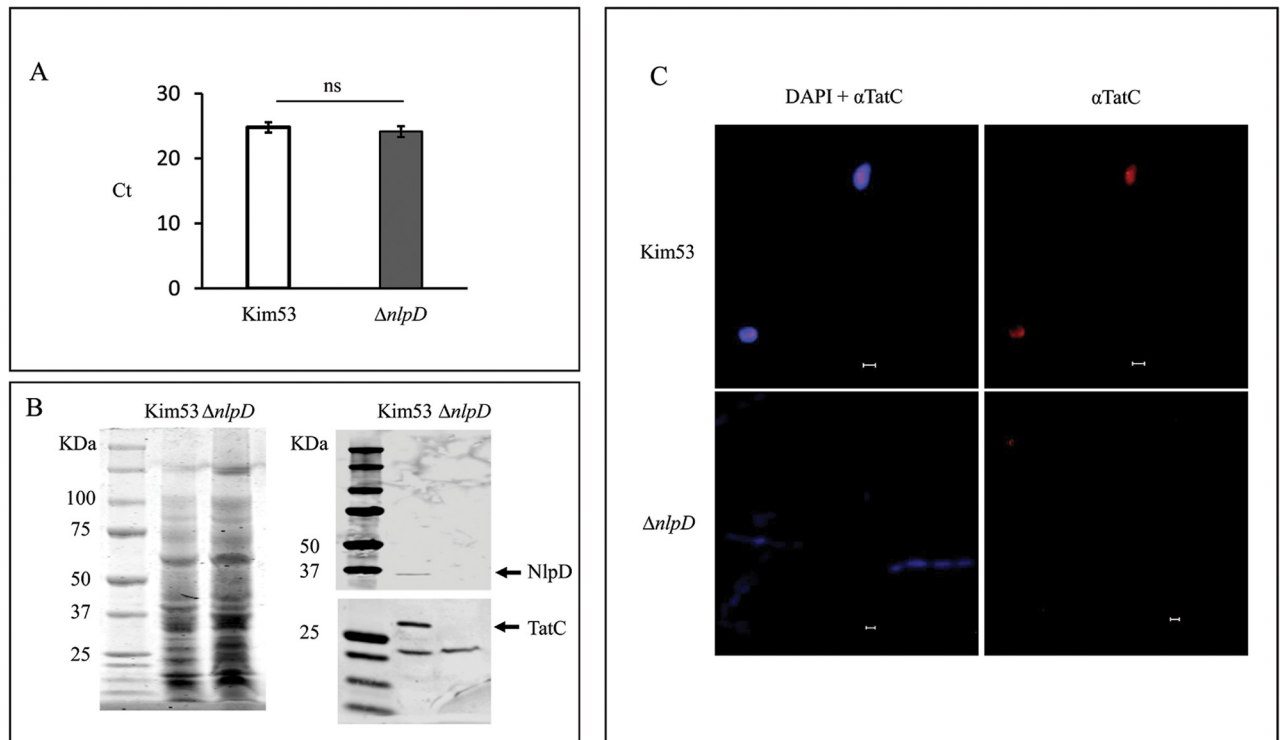


Fig 3. Expression of TatC in the *Y. pestis* strains. A. Quantitative RT-PCR analysis of *tatC* mRNA levels. mRNA from Kim53 (white histogram) and the *nlpD* mutant (gray histogram) was subjected to qRT-PCR analysis of *tatC* gene expression. The relative mRNA level was determined by calculating the threshold cycle (Δ Ct) of target genes via the classic Δ Ct method [90]. The results presented are an average of three independent experiments. B. Western blot analysis of TatC protein levels in total cell lysates of the wild-type Kim53 strain and the *nlpD* mutant. Whole cell lysates (10^6 cfu/lane grown at 37°C), were subjected to Western blot analysis using anti-NlpD and anti-TatC antibodies. The Coomassie blue stained gel and the blots were derived from the same experiment and were processed in parallel. C. Distribution of TatC protein on the bacterial membrane of *Y. pestis* strains. Fluorescence microscopy images of wild-type Kim53 (top panel) and the *nlpD* mutant (lower panel) are presented after TatC staining alone (right panel) or with DAPI staining (left panel). Images (100 \times) were captured with a Zeiss LSM 710 confocal microscope (Zeiss, Oberkochen, Germany). Scale bar = 1 μ m. The inset shows a magnification ($\times 3$) of stained bacterial cells. The data presented are representative of at least two independent experiments and the displayed data is one representative experiment.

<https://doi.org/10.1371/journal.pntd.0007449.g003>

Overall, these observations suggest that whereas the transcript levels of *tat* genes were not altered due to NlpD deletion, the *nlpD* mutant strain exhibited decreased levels of the Tat protein as indicated by monitoring TatC. These data raise the possibility that inactivation of the Tat system in the *nlpD* mutant could result from post-transcriptional events that affect proteins of the Tat machinery.

To verify that the loss of Tat functionality did not result from a general destabilization of the cytoplasmic membrane, the activity of Sec machinery, an additional inner-membrane imbedded transport system, was assessed. The Sec machinery is essential for the transport to the periplasm of the *Y. pestis* F1 capsular protein [64,65]. As depicted in Fig 4A, a similar distribution of the F1 protein was observed in the outer membrane of the wild-type strain and the *nlpD* mutant. In addition, the Sec pathway substrates BtuC and GadC were effectively expressed and transported to the periplasm of both wild-type and *nlpD* strains (Fig 4B and 4C), indicating that the Sec translocon is operational in the *nlpD* mutant in a similar manner to the wild-type strain. These results strongly suggest that the loss of Tat translocation activity in the *nlpD* mutant did not result from a general destabilization of the cytoplasmic membrane.

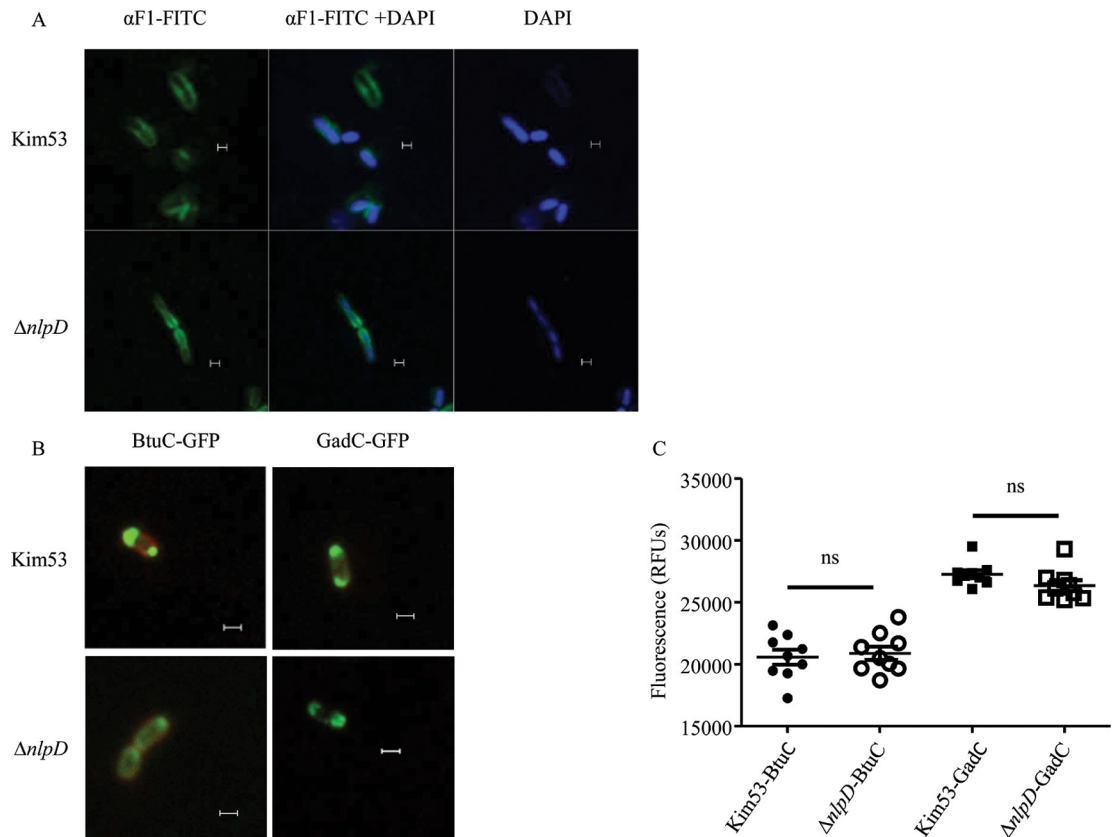


Fig 4. The Sec translocon is operational in the $\Delta nlpD$ mutant. A. The indicated bacterial cells were labeled with FITC-conjugated α -F1 antibodies (left), DAPI (right) or both α -F1 and DAPI (middle). B. Fluorescence microscopy of *Y. pestis* strains expressing the Sec-substrates BtuC and GadC fused to GFP. Scale bar = 1 μ m. C. Relative fluorescence units (RFUs) of the $\Delta nlpD$ mutant expressing BtuC-GFP or GadC-GFP, compared to the wild Kim53 strain expressing the reporter proteins, according to [40]. Ns, non-significant (Unpaired t test). The data presented are representative of at least two independent experiments and the displayed data in A and B is one representative experiment.

<https://doi.org/10.1371/journal.pntd.0007449.g004>

The *Y. pestis* mutants of the Tat system exhibit virulence attenuation and restricted growth under iron limiting conditions

As mentioned above, one of the major phenotypic characteristics of the *nlpD* mutant strain is its virulence attenuation. Therefore, we addressed the possibility that the NlpD associated effect on pathogenicity maybe attributed to the dysfunctionality of the Tat system. Indeed, it has been shown that the TatA protein is important for *Y. pestis* virulence in mouse models of plague [61]. Thus, we further addressed the attenuation of virulence and other phenotypic characteristics associated with the deletion of Tat proteins, in mutant strains exhibiting disruption of Tat genes in comparison to the phenotype exhibited by the *nlpD* mutated strain. Accordingly, the various mutants were characterized with respect to their morphology, iron acquisition capability and virulence in mouse models of plague.

Microscope analyses revealed a defect in cell segmentation of the *tatA* deletion mutant (Fig 5A). In addition, growth of the *tatA* and *tatC* mutants was severely inhibited under iron-limiting conditions in comparison to the wild-type strain, similar to the *nlpD* mutant (Fig 5Bi, Fig 1 and Table 2). Trans-complementation of the *nlpD*, *tatA* and *tatC* mutants with each of the corresponding genes (*nlpD* or *tatA* or *tatC*, respectively) was efficient in alleviating the growth under these conditions (Fig 5Bi and Table 2). Increasing the amounts of the iron chelator

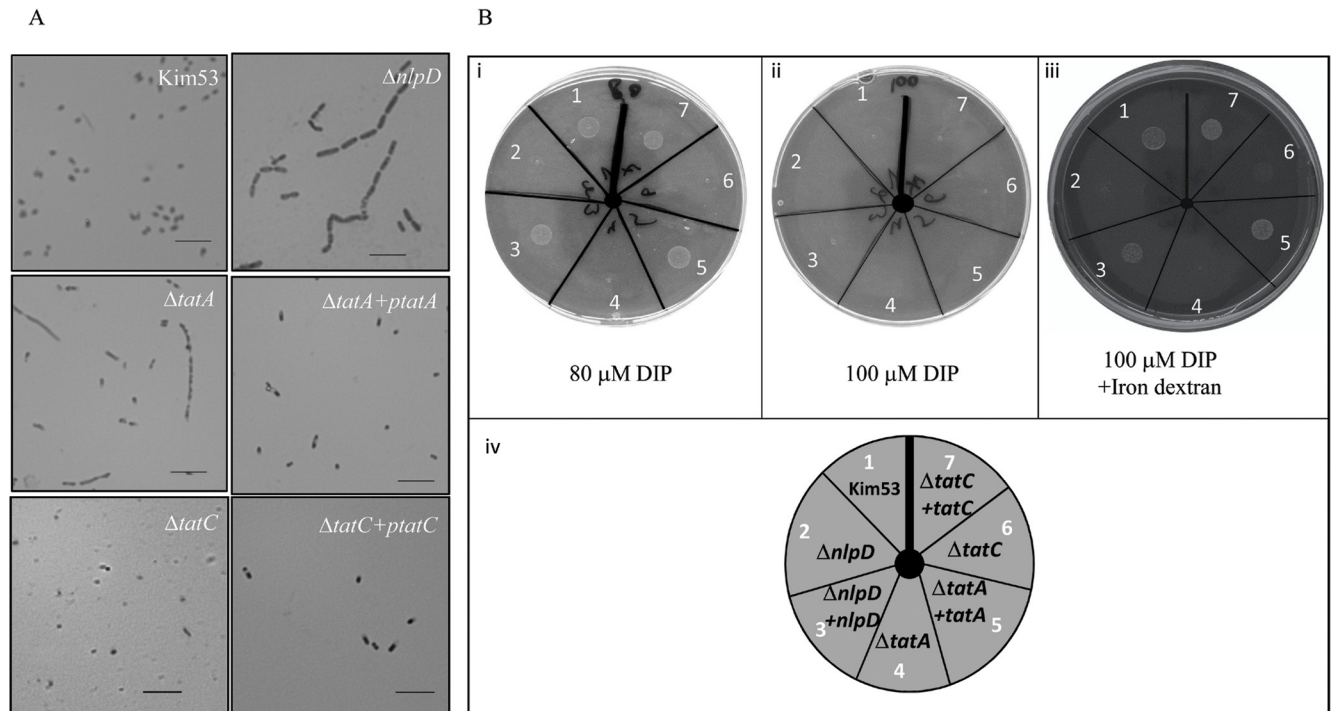


Fig 5. Phenotypic characterization of *Y. pestis* *tat* mutants. A. Gram staining of *Y. pestis* strains wild-type Kim53, $\Delta nlpD$, $\Delta tatA$, $\Delta tatC$, $\Delta tatA+ptatA$ and $\Delta tatC+ptatC$ was performed, and bacilli were observed by light microscopy at a magnification of $\times 1000$. Scale bar = 10 μm . B. Growth of *Y. pestis* strains under iron-limiting conditions. *Y. pestis* strains (see description in the lower panel, iv), were grown under iron-limiting conditions (see [Materials and Methods](#)). The medium included: 1% agarose, $1 \times PMH2$, 20 μM $MgCl_2$ and 80 μM DIP (i), 100 μM DIP (ii) or 100 μM DIP with addition of iron dextran (0.5mg/ml, iii). The displayed data is one representative experiment.

<https://doi.org/10.1371/journal.pntd.0007449.g005>

(DIP) to 100 μM resulted in growth inhibition of all *Y. pestis* strain (Fig 5Bii and Table 2). Addition of iron dextran (0.5mg/ml) to the plates containing the high concentration of DIP restored growth of the parental Kim53 strain as well as the trans-complemented *nlpD/pnlpD*, *tatA/ptatA* and *tatC/ptatC*, but not of *tatA*, *tatC* and *nlpD* mutants (Fig 5Biii and Table 2). Growth of the *tatA*, *tatC* and *nlpD* mutants was inhibited under iron limiting conditions and was not restored by addition of iron but only upon trans-complementation with the relevant gene (*nlpD* or *tatA* and *tatC* respectively, Fig 5Biii, Table 2).

Virulence of the *Y. pestis* *tat* mutants was evaluated in the well-established mouse models of bubonic and pneumonic plague [17,66]. As shown in Table 3, infection of CD-1 mice with

Table 2. Growth of *Y. pestis* strains under iron-limiting conditions.

Strain	Trans-complementation	Growth ^a		
		80 μg DIP	100 μg DIP	100 μg DIP + iron dextran
Kimberley53		+	-	++
Kim53 $\Delta nlpD$	-	-	-	-
Kim53 $\Delta nlpD$ pnlpD	<i>nlpD</i>	+	-	++
Kim53 $\Delta tatA$	-	-	-	-
Kim53 $\Delta tatA$ ptatA	<i>tatA</i>	+	-	++
Kim53 $\Delta tatC$	-	-	-	-
Kim53 $\Delta tatC$ ptatC	<i>tatC</i>	+	-	++

^a Growth under iron limiting conditions was evaluated on the basis of an arbitrary scale; accordingly, 3 levels of growth were defined: -, +, ++.

<https://doi.org/10.1371/journal.pntd.0007449.t002>

Table 3. Virulence of *Y. pestis* strains in mouse models of bubonic and pneumonic plague.

<i>Y. pestis</i> strain	LD ₅₀ value ^{a,b} (cfu)	
	s.c. route	i.n. route
Kimberley53	1–3	2,0 x10 ³
Kim53Δ <i>nlpD</i>	>2x10 ⁷	>4x10 ⁷
Kim53Δ <i>tatA</i>	>1x10 ⁷	>7x10 ⁶
Kim53Δ <i>tatC</i>	>5x10 ⁶	>5x10 ⁶
Kim53Δ <i>tatA ptatA</i>	<4	<4,4x10 ³
Kim53Δ <i>tatC ptatC</i>	<6	<4,8 x10 ³
Kim53Δ <i>amiC</i>	<3	<4,5 x10 ³

^aThe “<” symbol indicates that the calculated LD₅₀ value is the minimal infection dose tested, under which more than 50 percent of the animals died.

^bThe “>” symbol indicates that the calculated LD₅₀ value is the maximal infection dose tested under which less than 50 percent of the animals died.

<https://doi.org/10.1371/journal.pntd.0007449.t003>

high doses of the *tatA* mutant via the subcutaneous and intranasal routes was non-lethal. Furthermore, the *tatA* mutated bacteria could not be detected in the draining lymph node or the spleen of mice 48 hours after s.c. inoculation with high doses (10⁷ cfu/mouse), similar to the observations reported with respect to the *nlpD* mutated bacteria [20]. The results obtained with the s.c. administration of the TatA mutant are consistent with those of Bozue and colleagues [61], who showed that a *Y. pestis* CO92 *tatA* mutant was severely attenuated upon subcutaneous infection of Swiss Webster mice. As with the *nlpD* mutant (Fig 1B), the avirulent phenotype of the Kim53*tatA* mutant could not be reversed by exogenous administration of iron to the infected mice in line with the *in-vitro* growth results (Fig 5Biii). Yet, complementation by episomal expression of the *tatA* gene which restored the parental cell morphology and growth on iron-depleted medium (Fig 5 and Table 2) also reverted the virulent phenotype (Table 3), confirming that the observed phenotype is attributed to abrogation of TatA expression.

Of note, similar results to those pertaining to the TatA mutation could be obtained upon deletion of the *tatC* gene, including full restoration of the wild-type phenotype upon trans-complementation (morphology, Fig 5A, growth under iron deprivation, Fig 5B and virulence in the plague murine models, Table 3).

Taken together the data support the notion that the virulence attenuation characterizing the NlpD mutant phenotype maybe attributed to the dysfunctionality of the Tat system via a possible involvement in iron exploitation. This general possible explanation is compatible both with the micro-array transcriptomic data and the direct inspection of the Tat mutants.

Discussion

The lipoprotein NlpD emerged in a previous functional screen of *Y. pestis* genome as an important factor for the manifestation of *Y. pestis* virulence. The screen evidenced that NlpD gene disruption is incompatible with the survival of the bacteria in the host during infection [15,20]. In the current report, to gain further insight into the mechanisms underlying the role of NlpD in *Y. pestis* pathogenicity, the transcriptomes of the wild type Kim53 strain and the *nlpD* mutant were compared. Considering that the NlpD-mutated bacteria were rapidly cleared from inoculated animals [20], RNA for the transcriptome analysis was collected from bacteria cultured under conditions reminiscent of the initial stages of infection (growth of *Y. pestis* cultures at 37°C for several hours).

Examination of the differential transcriptome data clearly indicated that a pronounced membrane stress response is specifically induced in the *nlpD* mutant, as reflected by up-regulation of the *cpxP* and *pspA* genes (S2 Table). The Cpx and Psp systems are membrane stress-response pathways of Gram-negative bacteria that are involved in maintaining the homeostasis of the cytoplasmic membrane [43,44,67]. These systems sense and respond to periplasmic or cytoplasmic protein misfolding that disturb the integrity of the cytoplasmic membrane and could reduce the energy status of the cell [67,68,69,70]. In *Y. enterocolitica*, the Psp system has been shown to be essential for protecting bacterial cells against membrane damage due to miss-localization of the T3SS component secretin (YscC) that is induced at the mammalian body temperature of 37°C [71,72,73]. In the present study, *Y. pestis* cultures were grown at 37°C for five hours, resulting in induction of the T3SS [16]. However, inspection of the transcriptome data indicated that the expression of secretin was not differentially regulated in the *nlpD* mutant. The expression of only two T3SS components was altered in the *nlpD* mutant (S2 Table), the YscB chaperon that is required for the calcium-dependent regulation of Yop secretion [74] and YopQ (also known as YopK), which plays an important role in the regulation of Yops translocation [75].

The robust induction of Cpx and Psp stress response systems in the *nlpD* mutant suggests that in the absence of NlpD the integrity and/or stability of the membranes are affected and there is an increase in the accumulation of misfolded proteins in the periplasm. Interestingly, NlpE, which is another outer-membrane lipoprotein, is an accessory protein of the Cpx pathway in *E. coli* [76]. However, *nlpE* expression is not altered in the *nlpD* mutant compared with the wild-type strain. One may speculate that NlpD plays a similar role in responding to harmful changes that occur in bacterial membranes following exposure to environmental stress. Similarly, it has recently been demonstrated that changes in the peptidoglycan structure are part of the Cpx-mediated adaptation to envelope stress [77]. The proposed involvement of NlpD in the response to extracytoplasmic stress conditions is compatible with the genomic localization of the *nlpD* gene within a genomic stress response locus from which the SurE, Pcm and RpoS proteins are expressed [20].

Many of the differentially modulated pathways in the *nlpD* mutant were related to iron metabolism (~20%, S2 and S3 Tables), suggesting that the acquisition and consumption of iron may have been perturbed by NlpD deletion. The hypothesis that the mutated cells have an impaired ability to exploit iron was further confirmed by the observation that the mutated bacterial cells failed to grow under iron-limiting conditions (Fig 1A). Lowering the levels of free iron is an important host defense strategy that restricts the proliferation of infectious bacteria [78,79], and many pathogens have evolved sophisticated mechanisms to overcome this restriction and maximize the host iron supply [78,80]. Accordingly, we have recently shown that the *Y. pestis* EV76 live vaccine protected mice against an immediate lethal challenge with a virulent *Y. pestis* strain and that protection was associated with induction of the host heme- and iron-binding proteins hemopexin and transferrin [81].

Close inspection and integration of all the observed phenotypic characteristics of the *Y. pestis nlpD* mutant, namely, chain-forming morphology, attenuation of virulence, reduced tolerance to acidic stress, defective iron acquisition and envelope stresses, suggested a striking resemblance to the phenotypic characteristics of bacterial Tat mutants in other pathogens [52,53]. Importantly, similar to the situation of the *Y. pestis nlpD* mutant, the loss of virulence of *Yersinia* Tat mutated strains could not be explained by the dysfunction of the T3SS [60,61].

The assumption that the Tat system is impaired in the *nlpD* mutant was supported by the observed decrease in the expression of several known iron-sulfur protein substrates of this system (S2 Table). In addition, the modulation of type VI secretion system genes observed in the *nlpD* mutant (S2 Table) was also observed in Tat mutants of the phylogenetically related strain

Y. pseudotuberculosis [82], and the fish pathogen *E. tarda* [83]. Furthermore, although *Y. pestis* is a non-motile bacterium, a flagellar operon was modulated in the *nlpD* mutant (S2 Table), suggesting a possible control on motility that characterize Tat mutants in many bacterial pathogens including *Y. pseudotuberculosis* [52,59,60]. The assumption that the phenotype of the NlpD mutant is related to deregulation of the Tat system was directly interrogated. Assessment of the functionality of the Tat system in the *nlpD* mutant was performed by visualization (using microscope analysis and confirmed by subcellular fractionation analysis) of the localization of two different Tat reporter substrates: a GFP-reporter protein fused to the signal peptide of the Tat-substrate TorA or the Tat-substrate NapG [25,60,62]. As hypothesized, the Tat system was not functional in the *Y. pestis nlpD* mutant (Fig 2), whereas other translocation systems including the inner-membrane embedded Sec pathway (Fig 4), and the T3SS that traverse the inner and outer membrane of the cell [20], were operational in the *nlpD* mutant indistinguishably from the wild-type strain. These observations suggested that inactivation of the Tat system in the *nlpD* mutant did not result from a general destabilization of the bacterial membrane and substantiate the specificity of the phenotype exhibited by the *nlpD* mutant strain.

TatC protein levels (Fig 3B) as well as the membrane localization of this protein (Fig 3C) confirmed that the Tat system is affected in the *nlpD* mutant. The TatC protein level in cell lysates of the *nlpD* mutant was decreased in comparison to the wild-type strain, and this protein was not detected in the mutant cytoplasmic membrane. Since the RNA levels of the Tat genes were similar in wild-type and the *nlpD* mutant, one may speculate that dysfunction of the Tat system in the *nlpD* mutant could have resulted from post-transcriptional molecular events. In *Y. pseudotuberculosis*, a *tatC* mutant was highly attenuated for virulence following oral or intraperitoneal infections [60]. The system was important for different virulence-related stress responses as well as for iron uptake [60]. Additional studies have indicated that the loss of virulence is related to the SufI Tat-substrate that was found to be required for establishment of systemic infection [84].

The *Y. pestis tatA* and *tatC* mutants were avirulent in mice. In *Y. pestis* CO92, the *tatA* mutant was highly attenuated in the bubonic and aerosol-infection mouse model but to a lesser extent in the intranasal infection model [61]. Attenuation of virulence in the bubonic plague model is therefore similar in both *Y. pestis tatA* mutant strains. The differences between the virulence characteristics of the Kim53 and CO92 *tatA* mutants in the i.n. infection model may reflect variations in the mouse strain used for the evaluation of virulence or the genetic diversity between the two *Y. pestis* strains.

The known functions of the NlpD lipoprotein, which belong to the M23-LytM endopeptidase family, involves the regulation of peptidoglycan hydrolysis and cell morphogenesis [20,21,85,86]. In *E. coli*, the NlpD protein is not catalytically active but controls the activity and recruitment to the septum of the cell wall amidase—AmiC, which is a known Tat system substrate [85,87,88,89]. Interestingly, the *Y. pestis amiC* mutant retained the wild-type single cell morphology (S7 Fig) and virulence characteristics (Table 3). These observations suggest that in *Y. pestis* the mode of interactions between NlpD and AmiC maybe different than in *E. coli*.

The present study shows that the *nlpD* mutant exhibited impaired Tat activity as well as limited iron acquisition. Both of these characteristics may have represented the cause for the severe virulence attenuation exhibited by the *nlpD* mutant. Considering the similarity between the phenotypic characteristics of the *nlpD* mutant and the *tat* mutants including chain morphology, iron assimilation defect and loss of virulence, the present data suggest a novel link between NlpD and the Tat system affecting *Y. pestis* pathogenesis.

The molecular mechanisms underlying the possible relationships between NlpD, the Tat system components and iron assimilation remain to be deciphered and raise several questions

including the possible interactions between the outer membrane-predicted NlpD lipoprotein, and iron assimilation systems or the inner membrane Tat proteins. Studies addressing some of these issues are currently underway in our laboratory.

Supporting information

S1 Fig. Expression of TatC, NlpD and Pcm in *Y. pestis* tat mutants. A. Coomassie blue stain (upper panel) and Western blot analysis of TatC and NlpD protein levels in total cell lysates (lower panel). Cultures of *Y. pestis* strains were inoculated (initial OD₆₆₀ = 0.01) and incubated for an additional 24 hours at 37°C. Western blot analysis was performed with anti-NlpD, anti-TatC and anti-Pcm antibodies, to equal amount of cells/lane. The Pcm protein served as loading control. Coomassie blue stained gel and the blots were derived from the same experiment and were processed in parallel. B. The original uncropped Western blots depicted in A. The portions of the Western blots used in panel A, are indicated by black rectangles.

(TIF)

S2 Fig. Differentially expressed genes in *Y. pestis* nlpD mutant relative to the parental Kim53 strain. A graphical presentation of the fold changes of up-regulated (A) or down-regulate (B) genes in the *nlpD* mutant relative to the wild-type Kim53 strain. The genes are categorized according to their functional classification (see S2, S3, S4 and S5 Tables).

(TIF)

S3 Fig. Comparison of transcription measurements by microarray and real-time PCR assays. The relative transcriptional levels of the genes were determined by real-time RT-PCR. The log₂ values were plotted against the microarray data log₂ values. The correlation coefficient (R²) for comparison of the two datasets is 0.8459.

(TIF)

S4 Fig. Intracellular localization of the NapG-GFP Tat-reporter protein in *Y. pestis* strains. *Y. pestis* strains: Kim53p:*napG*:GFP, Kim53Δ*nlpD*:*napG*:GFP and Kim53Δ*nlpD*+*pnlpD*:*napG*:GFP were inspected under a fluorescence microscope for identification of NapG-GFP (Tat substrate protein fused to GFP) localization. The scale bar represents 1 μm.

(TIF)

S5 Fig. Original uncropped Western blots depicted in Fig 2B. See legend to Fig 2. The original uncropped Western blots depicted in Fig 2B. The portions of the Western blots used are indicated by black rectangles. *The *tatB* mutant is not presented in Fig 2 due to a polar effect caused by *tatB* deletion that tampered TatC expression.

(TIF)

S6 Fig. Original uncropped Western blots depicted in Fig 3B. See legend to Fig 3. The portions of the coomassie stained gel and the Western blots used are indicated by black rectangles.

(TIF)

S7 Fig. Phenotypic characterization of *Y. pestis* Kim53Δ*amiC* strain. Gram staining of *Y. pestis* Δ*amiC* mutant was performed. Bacilli were observed by light microscopy at a magnification of ×1000. Scale bar = 10 μm.

(TIF)

S1 Table. Primers used in this study.

(DOCX)

S2 Table. Genes up-regulated in *Y. pestis nlpD* mutant relative to the parental Kim53 strain.

(DOCX)

S3 Table. Genes down-regulated in *Y. pestis nlpD* mutant relative to the parental Kim53 strain.

(DOCX)

S4 Table. Excel file specifying the up-regulated YPO gene numbers.

(XLSX)

S5 Table. Excel file specifying the down-regulated YPO gene numbers.

(XLSX)

S6 Table. qRT-PCR-determined differentially expressed genes.

(DOCX)

Acknowledgments

We gratefully thank Dr. [Jacqueline Fetherston](#) and Dr. Robert Perry for contributing valuable advice regarding growth of *Y. pestis* strains in iron limiting conditions and to Professor Eitan Bibi for providing the ORF clones of *Escherichia coli* ASKA library. We would also wish to thank Dr. Avigdor Shafferman for fruitful scientific discussions.

Author Contributions

Conceptualization: Avital Tidhar, Yehuda Flashner, Emanuelle Mamroud.

Data curation: Avital Tidhar, Theodor Chitlaru, Emanuelle Mamroud.

Formal analysis: Avital Tidhar, Naomi Ariel, Emanuelle Mamroud.

Funding acquisition: Emanuelle Mamroud.

Investigation: Avital Tidhar, Yinon Levy, Ayelet Zauberman, Yaron Vagima, David Gur, Moshe Aftalion, Ofir Israeli, Yehuda Flashner, Emanuelle Mamroud.

Methodology: Avital Tidhar, Yinon Levy, Ayelet Zauberman, Yaron Vagima, David Gur, Moshe Aftalion, Anat Zvi, Emanuelle Mamroud.

Project administration: Emanuelle Mamroud.

Software: Naomi Ariel, Anat Zvi.

Supervision: Emanuelle Mamroud.

Validation: Avital Tidhar, Yinon Levy, Ayelet Zauberman, Yaron Vagima, David Gur, Moshe Aftalion, Ofir Israeli, Naomi Ariel, Anat Zvi, Emanuelle Mamroud.

Visualization: Avital Tidhar, Emanuelle Mamroud.

Writing – original draft: Avital Tidhar, Theodor Chitlaru, Emanuelle Mamroud.

Writing – review & editing: Avital Tidhar, Theodor Chitlaru, Emanuelle Mamroud.

References

1. Seshasayee AS, Bertone P, Fraser GM, Luscombe NM (2006) Transcriptional regulatory networks in bacteria: from input signals to output responses. *Curr Opin Microbiol* 9: 511–519. <https://doi.org/10.1016/j.mib.2006.08.007> PMID: 16942903

2. Perry RD, Fetherston JD (1997) *Yersinia pestis*—etiologic agent of plague. *Clin Microbiol Rev* 10: 35–66. PMID: [8993858](#)
3. Bertherat J (2016) The Challenge of Early Diagnosis of Cushing Disease Recurrence! *Endocr Pract* 22: 1356–1357. <https://doi.org/10.4158/EP161600.CO> PMID: [27749130](#)
4. Simond P (1905) La question du véhicule de la peste. *Re Me'dico-Chirurg Bre'sil Am Lat* (5).
5. Simond M, Godley ML, Mouriquand PD (1998) Paul-Louis Simond and his discovery of plague transmission by rat fleas: a centenary. *J R Soc Med* 91: 101–104. PMID: [9602755](#)
6. Inglesby TV, Dennis DT, Henderson DA, Bartlett JG, Ascher MS, et al. (2000) Plague as a biological weapon: medical and public health management. Working Group on Civilian Biodefense. *JAMA* 283: 2281–2290. PMID: [10807389](#)
7. Ke Y, Chen Z, Yang R (2013) *Yersinia pestis*: mechanisms of entry into and resistance to the host cell. *Front Cell Infect Microbiol* 3: 106. <https://doi.org/10.3389/fcimb.2013.00106> PMID: [24400226](#)
8. Heroven AK, Dersch P (2014) Coregulation of host-adapted metabolism and virulence by pathogenic yersiniae. *Front Cell Infect Microbiol* 4: 146. <https://doi.org/10.3389/fcimb.2014.00146> PMID: [25368845](#)
9. Perry RD, Fetherston JD (2011) Yersiniabactin iron uptake: mechanisms and role in *Yersinia pestis* pathogenesis. *Microbes Infect* 13: 808–817. <https://doi.org/10.1016/j.micinf.2011.04.008> PMID: [21609780](#)
10. Brubaker RR, Beesley ED, Surgalla MJ (1965) *Pasteurella pestis*: Role of Pesticin I and Iron in Experimental Plague. *Science* 149: 422–424. <https://doi.org/10.1126/science.149.3682.422> PMID: [17809405](#)
11. Lathem WW, Price PA, Miller VL, Goldman WE (2007) A plasminogen-activating protease specifically controls the development of primary pneumonic plague. *Science* 315: 509–513. <https://doi.org/10.1126/science.1137195> PMID: [17255510](#)
12. Hinnebusch BJ, Jarrett CO, Callison JA, Gardner D, Buchanan SK, et al. (2011) Role of the *Yersinia pestis* Ail protein in preventing a protective polymorphonuclear leukocyte response during bubonic plague. *Infect Immun* 79: 4984–4989. <https://doi.org/10.1128/IAI.05307-11> PMID: [21969002](#)
13. Cathelyn JS, Crosby SD, Lathem WW, Goldman WE, Miller VL (2006) RovA, a global regulator of *Yersinia pestis*, specifically required for bubonic plague. *Proc Natl Acad Sci U S A* 103: 13514–13519. <https://doi.org/10.1073/pnas.0603456103> PMID: [16938880](#)
14. Cornelis GR, Boland A, Boyd AP, Geuijen C, Iriarte M, et al. (1998) The virulence plasmid of *Yersinia*, an antihost genome. *Microbiol Mol Biol Rev* 62: 1315–1352. PMID: [9841674](#)
15. Flashner Y, Mamroud E, Tidhar A, Ber R, Aftalion M, et al. (2004) Generation of *Yersinia pestis* attenuated strains by signature-tagged mutagenesis in search of novel vaccine candidates. *Infect Immun* 72: 908–915. <https://doi.org/10.1128/IAI.72.2.908-915.2004> PMID: [14742535](#)
16. Zauberman A, Cohen S, Mamroud E, Flashner Y, Tidhar A, et al. (2006) Interaction of *Yersinia pestis* with macrophages: limitations in YopJ-dependent apoptosis. *Infect Immun* 74: 3239–3250. <https://doi.org/10.1128/IAI.00097-06> PMID: [16714551](#)
17. Vagima Y, Zauberman A, Levy Y, Gur D, Tidhar A, et al. (2015) Circumventing *Y. pestis* Virulence by Early Recruitment of Neutrophils to the Lungs during Pneumonic Plague. *PLoS Pathog* 11: e1004893. <https://doi.org/10.1371/journal.ppat.1004893> PMID: [25974210](#)
18. Palace SG, Proulx MK, Lu S, Baker RE, Goguen JD (2014) Genome-wide mutant fitness profiling identifies nutritional requirements for optimal growth of *Yersinia pestis* in deep tissue. *MBio* 5.
19. Li B, Yang R (2008) Interaction between *Yersinia pestis* and the Host Immune System. *INFECTION AND IMMUNITY* 76: 1804–1811.
20. Tidhar A, Flashner Y, Cohen S, Levi Y, Zauberman A, et al. (2009) The NlpD lipoprotein is a novel *Yersinia pestis* virulence factor essential for the development of plague. *PLoS One* 4: e7023. <https://doi.org/10.1371/journal.pone.0007023> PMID: [19759820](#)
21. Uehara T, Dinh T, Bernhardt TG (2009) LytM-domain factors are required for daughter cell separation and rapid ampicillin-induced lysis in *Escherichia coli*. *J Bacteriol* 191: 5094–5107. <https://doi.org/10.1128/JB.00505-09> PMID: [19525345](#)
22. Ercoli G, Tani C, Pezzicoli A, Vacca I, Martinelli M, et al. (2015) LytM proteins play a crucial role in cell separation, outer membrane composition, and pathogenesis in nontypeable *Haemophilus influenzae*. *MBio* 6: e02575. <https://doi.org/10.1128/mBio.02575-14> PMID: [25714719](#)
23. Berks BC, Palmer T, Sargent F (2005) Protein targeting by the bacterial twin-arginine translocation (Tat) pathway. *Curr Opin Microbiol* 8: 174–181. <https://doi.org/10.1016/j.mib.2005.02.010> PMID: [15802249](#)

24. Ben-Gurion R, Shafferman A (1981) Essential virulence determinants of different *Yersinia* species are carried on a common plasmid. *Plasmid* 5: 183–187. PMID: [7243971](#)
25. Craig M, Sadik AY, Golubeva YA, Tidhar A, Slauch JM (2013) Twin-arginine translocation system (tat) mutants of *Salmonella* are attenuated due to envelope defects, not respiratory defects. *Mol Microbiol* 89: 887–902. <https://doi.org/10.1111/mmi.12318> PMID: [23822642](#)
26. Kitagawa M, Ara T, Arifuzzaman M, Ioka-Nakamichi T, Inamoto E, et al. (2005) Complete set of ORF clones of *Escherichia coli* ASKA library (a complete set of *E. coli* K-12 ORF archive): unique resources for biological research. *DNA Res* 12: 291–299. <https://doi.org/10.1093/dnares/dsi012> PMID: [16769691](#)
27. Datsenko KA, Wanner BL (2000) One-step inactivation of chromosomal genes in *Escherichia coli* K-12 using PCR products. *Proc Natl Acad Sci U S A* 97: 6640–6645. <https://doi.org/10.1073/pnas.120163297> PMID: [10829079](#)
28. Wang RF, Kushner SR (1991) Construction of versatile low-copy-number vectors for cloning, sequencing and gene expression in *Escherichia coli*. *Gene* 100: 195–199. PMID: [2055470](#)
29. Kirillina O, Bobrov AG, Fetherston JD, Perry RD (2006) Hierarchy of iron uptake systems: Yfu and Yiu are functional in *Yersinia pestis*. *Infect Immun* 74: 6171–6178. <https://doi.org/10.1128/IAI.00874-06> PMID: [16954402](#)
30. Staggs TM, Perry RD (1991) Identification and cloning of a fur regulatory gene in *Yersinia pestis*. *J Bacteriol* 173: 417–425. <https://doi.org/10.1128/jb.173.2.417-425.1991> PMID: [1898928](#)
31. Gong S, Bearden SW, Geoffroy VA, Fetherston JD, Perry RD (2001) Characterization of the *Yersinia pestis* Yfu ABC inorganic iron transport system. *Infect Immun* 69: 2829–2837. <https://doi.org/10.1128/IAI.67.5.2829-2837.2001> PMID: [11292695](#)
32. Lucier TS, Fetherston JD, Brubaker RR, Perry RD (1996) Iron uptake and iron-repressible polypeptides in *Yersinia pestis*. *Infect Immun* 64: 3023–3031. PMID: [8757829](#)
33. Steinberger-Levy I, Shifman O, Zvi A, Ariel N, Beth-Din A, et al. (2016) A Rapid Molecular Test for Determining *Yersinia pestis* Susceptibility to Ciprofloxacin by the Quantification of Differentially Expressed Marker Genes. *Front Microbiol* 7: 763. <https://doi.org/10.3389/fmicb.2016.00763> PMID: [27242774](#)
34. Smyth GK, Yang YH, Speed T (2003) Statistical issues in cDNA microarray data analysis. *Methods Mol Biol* 224: 111–136. <https://doi.org/10.1385/1-59259-364-X:111> PMID: [12710670](#)
35. Benjamini Y, Hochberg Y (1995) Controlling the false discovery rate: a practical and powerful approach to multiple testing. *Journal of the Royal Statistical Society Series B (Methodological)* 57: 289–300.
36. Klipper-Aurbach Y, Wasserman M, Braunspeigel-Weintrob N, Borstein D, Peleg S, et al. (1995) Mathematical formulae for the prediction of the residual beta cell function during the first two years of disease in children and adolescents with insulin-dependent diabetes mellitus. *Med Hypotheses* 45: 486–490. PMID: [8748093](#)
37. Levy Y, Flashner Y, Tidhar A, Zauberman A, Aftalion M, et al. (2011) T cells play an essential role in anti-F1 mediated rapid protection against bubonic plague. *Vaccine* 29: 6866–6873. <https://doi.org/10.1016/j.vaccine.2011.07.059> PMID: [21803090](#)
38. Mechaly A, Vitner E, Levy H, Weiss S, Bar-David E, et al. (2018) Simultaneous Immunodetection of Anthrax, Plague, and Tularemia from Blood Cultures by Use of Multiplexed Suspension Arrays. *J Clin Microbiol* 56.
39. Alcock F, Damen MP, Levring J, Berks BC (2017) In vivo experiments do not support the charge zipper model for Tat translocase assembly. *Elife* 6.
40. Yosef I, Bochkareva ES, Bibi E (2010) *Escherichia coli* SRP, its protein subunit Ffh, and the Ffh M domain are able to selectively limit membrane protein expression when overexpressed. *MBio* 1.
41. Levy Y, Vagima Y, Tidhar A, Zauberman A, Aftalion M, et al. (2016) Adjunctive Corticosteroid Treatment Against *Yersinia pestis* Improves Bacterial Clearance, Immunopathology, and Survival in the Mouse Model of Bubonic Plague. *J Infect Dis* 214: 970–977. <https://doi.org/10.1093/infdis/jiw290> PMID: [27402776](#)
42. Reed LJM H. (1938) A simple method of estimating fifty percent endpoints. *The American Journal of Hygiene* 5.
43. Joly N, Engl C, Jovanovic G, Huvet M, Toni T, et al. (2010) Managing membrane stress: the phage shock protein (Psp) response, from molecular mechanisms to physiology. *FEMS Microbiol Rev* 34: 797–827. <https://doi.org/10.1111/j.1574-6976.2010.00240.x> PMID: [20636484](#)
44. Raivio TL (2014) Everything old is new again: an update on current research on the Cpx envelope stress response. *Biochim Biophys Acta* 1843: 1529–1541. <https://doi.org/10.1016/j.bbamcr.2013.10.018> PMID: [24184210](#)
45. Skaar EP (2010) The battle for iron between bacterial pathogens and their vertebrate hosts. *PLoS Pathog* 6: e1000949. <https://doi.org/10.1371/journal.ppat.1000949> PMID: [20711357](#)

46. Fetherston JD, Kirillina O, Bobrov AG, Paulley JT, Perry RD (2010) The yersiniabactin transport system is critical for the pathogenesis of bubonic and pneumonic plague. *Infect Immun* 78: 2045–2052. <https://doi.org/10.1128/IAI.01236-09> PMID: 20160020
47. Perry RD, Balbo PB, Jones HA, Fetherston JD, DeMoll E (1999) Yersiniabactin from *Yersinia pestis*: biochemical characterization of the siderophore and its role in iron transport and regulation. *Microbiology* 145 (Pt 5): 1181–1190.
48. Schwartz CJ, Giel JL, Patschkowski T, Luther C, Ruzicka FJ, et al. (2001) IscR, an Fe-S cluster-containing transcription factor, represses expression of *Escherichia coli* genes encoding Fe-S cluster assembly proteins. *Proc Natl Acad Sci U S A* 98: 14895–14900. <https://doi.org/10.1073/pnas.251550898> PMID: 11742080
49. Ren Q, Ahuja U, Thony-Meyer L (2002) A bacterial cytochrome c heme lyase. CcmF forms a complex with the heme chaperone CcmE and CcmH but not with apocytochrome c. *J Biol Chem* 277: 7657–7663. <https://doi.org/10.1074/jbc.M110979200> PMID: 11744735
50. Messenger Ann J M, Barclay R (1983) Bacteria, iron and pathogenicity. *Biochemistry and Molecular Biology Education* 11: 10.
51. Galvan EM, Nair MK, Chen H, Del Piero F, Schifferli DM (2010) Biosafety level 2 model of pneumonic plague and protection studies with F1 and Psa. *Infect Immun* 78: 3443–3453. <https://doi.org/10.1128/IAI.00382-10> PMID: 20498260
52. De Buck E, Lammertyn E, Anne J (2008) The importance of the twin-arginine translocation pathway for bacterial virulence. *Trends Microbiol* 16: 442–453. <https://doi.org/10.1016/j.tim.2008.06.004> PMID: 18715784
53. Palmer T, Sargent F, Berks BC (2005) Export of complex cofactor-containing proteins by the bacterial Tat pathway. *Trends Microbiol* 13: 175–180. <https://doi.org/10.1016/j.tim.2005.02.002> PMID: 15817387
54. Weiner JH, Bilous PT, Shaw GM, Lubitz SP, Frost L, et al. (1998) A novel and ubiquitous system for membrane targeting and secretion of cofactor-containing proteins. *Cell* 93: 93–101. PMID: 9546395
55. Lee PA, Tullman-Ercek D, Georgiou G (2006) The bacterial twin-arginine translocation pathway. *Annu Rev Microbiol* 60: 373–395. <https://doi.org/10.1146/annurev.micro.60.080805.142212> PMID: 16756481
56. Chaddock AM, Mant A, Karnauchova I, Brink S, Herrmann RG, et al. (1995) A new type of signal peptide: central role of a twin-arginine motif in transfer signals for the delta pH-dependent thylakoidal protein translocase. *EMBO J* 14: 2715–2722. PMID: 7796800
57. Berks BC (1996) A common export pathway for proteins binding complex redox cofactors? *Mol Microbiol* 22: 393–404. <https://doi.org/10.1046/j.1365-2958.1996.00114.x> PMID: 8939424
58. Robinson C, Bolhuis A (2001) Protein targeting by the twin-arginine translocation pathway. *Nat Rev Mol Cell Biol* 2: 350–356. <https://doi.org/10.1038/35073038> PMID: 11331909
59. Ochsner UA, Snyder A, Vasil AI, Vasil ML (2002) Effects of the twin-arginine translocase on secretion of virulence factors, stress response, and pathogenesis. *Proc Natl Acad Sci U S A* 99: 8312–8317. <https://doi.org/10.1073/pnas.082238299> PMID: 12034867
60. Lavander M, Ericsson SK, Broms JE, Forsberg A (2006) The twin arginine translocation system is essential for virulence of *Yersinia pseudotuberculosis*. *Infect Immun* 74: 1768–1776. <https://doi.org/10.1128/IAI.74.3.1768-1776.2006> PMID: 16495550
61. Bozue J, Cote CK, Chance T, Kugelman J, Kern SJ, et al. (2014) A *Yersinia pestis* tat mutant is attenuated in bubonic and small-aerosol pneumonic challenge models of infection but not as attenuated by intranasal challenge. *PLoS One* 9: e104524. <https://doi.org/10.1371/journal.pone.0104524> PMID: 25101850
62. Thomas JD, Daniel RA, Errington J, Robinson C (2001) Export of active green fluorescent protein to the periplasm by the twin-arginine translocase (Tat) pathway in *Escherichia coli*. *Mol Microbiol* 39: 47–53. PMID: 11123687
63. Palmer T, Berks BC, Sargent F (2010) Analysis of Tat targeting function and twin-arginine signal peptide activity in *Escherichia coli*. *Methods Mol Biol* 619: 191–216. https://doi.org/10.1007/978-1-60327-412-8_12 PMID: 20419412
64. Zavialov AV, Berglund J, Pudney AF, Fooks LJ, Ibrahim TM, et al. (2003) Structure and biogenesis of the capsular F1 antigen from *Yersinia pestis*: preserved folding energy drives fiber formation. *Cell* 113: 587–596. PMID: 12787500
65. Knight SD (2007) Structure and assembly of *Yersinia pestis* F1 antigen. *Adv Exp Med Biol* 603: 74–87. https://doi.org/10.1007/978-0-387-72124-8_6 PMID: 17966405

66. Zauberman A, Flashner Y, Levy Y, Vagima Y, Tidhar A, et al. (2013) YopP-expressing variant of *Y. pestis* activates a potent innate immune response affording cross-protection against yersiniosis and tularemia [corrected]. *PLoS One* 8: e83560. <https://doi.org/10.1371/journal.pone.0083560> PMID: 24358292
67. Grabowicz M, Silhavy TJ (2017) Envelope Stress Responses: An Interconnected Safety Net. *Trends Biochem Sci* 42: 232–242. <https://doi.org/10.1016/j.tibs.2016.10.002> PMID: 27839654
68. Isaac DD, Pinkner JS, Hultgren SJ, Silhavy TJ (2005) The extracytoplasmic adaptor protein CpxP is degraded with substrate by DegP. *Proc Natl Acad Sci U S A* 102: 17775–17779. <https://doi.org/10.1073/pnas.0508936102> PMID: 16303867
69. Hunke S, Keller R, Muller VS (2012) Signal integration by the Cpx-envelope stress system. *FEMS Microbiol Lett* 326: 12–22. <https://doi.org/10.1111/j.1574-6968.2011.02436.x> PMID: 22092888
70. Yamaguchi S, Gueguen E, Horstman NK, Darwin AJ (2010) Membrane association of PspA depends on activation of the phage-shock-protein response in *Yersinia enterocolitica*. *Mol Microbiol* 78: 429–443. PMID: 20979344
71. Yamaguchi S, Darwin AJ (2012) Recent findings about the *Yersinia enterocolitica* phage shock protein response. *J Microbiol* 50: 1–7. <https://doi.org/10.1007/s12275-012-1578-7> PMID: 22367931
72. Chen S, Thompson KM, Francis MS (2016) Environmental Regulation of *Yersinia* Pathophysiology. *Front Cell Infect Microbiol* 6: 25. <https://doi.org/10.3389/fcimb.2016.00025> PMID: 26973818
73. Darwin AJ, Miller VL (2001) The *psp* locus of *Yersinia enterocolitica* is required for virulence and for growth in vitro when the Ysc type III secretion system is produced. *Mol Microbiol* 39: 429–444. PMID: 11136463
74. Joseph SS, Plano GV (2013) The SycN/YscB chaperone-binding domain of YopN is required for the calcium-dependent regulation of Yop secretion by *Yersinia pestis*. *Front Cell Infect Microbiol* 3: 1. <https://doi.org/10.3389/fcimb.2013.00001> PMID: 23355975
75. Dewoody R, Merritt PM, Houppert AS, Marketon MM (2011) YopK regulates the *Yersinia pestis* type III secretion system from within host cells. *Mol Microbiol* 79: 1445–1461. <https://doi.org/10.1111/j.1365-2958.2011.07534.x> PMID: 21205017
76. Snyder WB, Davis LJ, Danese PN, Cosma CL, Silhavy TJ (1995) Overproduction of NlpE, a new outer membrane lipoprotein, suppresses the toxicity of periplasmic LacZ by activation of the Cpx signal transduction pathway. *J Bacteriol* 177: 4216–4223. <https://doi.org/10.1128/jb.177.15.4216-4223.1995> PMID: 7635808
77. Bernal-Cabas M, Ayala JA, Raivio TL (2015) The Cpx envelope stress response modifies peptidoglycan cross-linking via the L,D-transpeptidase LdtD and the novel protein YgaU. *J Bacteriol* 197: 603–614. <https://doi.org/10.1128/JB.02449-14> PMID: 25422305
78. Cassat JE, Skaar EP (2013) Iron in infection and immunity. *Cell Host Microbe* 13: 509–519. <https://doi.org/10.1016/j.chom.2013.04.010> PMID: 23684303
79. Weinberg ED (1975) Nutritional immunity. Host's attempt to withhold iron from microbial invaders. *JAMA* 231: 39–41. PMID: 1243565
80. Parrow NL, Fleming RE, Minnick MF (2013) Sequestration and scavenging of iron in infection. *Infect Immun* 81: 3503–3514. <https://doi.org/10.1128/IAI.00602-13> PMID: 23836822
81. Zauberman A, Vagima Y, Tidhar A, Aftalion M, Gur D, et al. (2017) Host Iron Nutritional Immunity Induced by a Live *Yersinia pestis* Vaccine Strain Is Associated with Immediate Protection against Plague. *Front Cell Infect Microbiol* 7: 277. <https://doi.org/10.3389/fcimb.2017.00277> PMID: 28680860
82. Avican U, Beckstette M, Heroven AK, Lavander M, Dersch P, et al. (2016) Transcriptomic and Phenotypic Analysis Reveals New Functions for the Tat Pathway in *Yersinia pseudotuberculosis*. *J Bacteriol* 198: 2876–2886. <https://doi.org/10.1128/JB.00352-16> PMID: 27501981
83. Wang Y, Wang Q, Yang M, Zhang Y (2013) Proteomic analysis of a twin-arginine translocation-deficient mutant unravel its functions involved in stress adaptation and virulence in fish pathogen *Edwardsiella tarda*. *FEMS Microbiol Lett* 343: 145–155. <https://doi.org/10.1111/1574-6968.12140> PMID: 23551118
84. Avican U, Doruk T, Ostberg Y, Fahlgren A, Forsberg A (2017) The Tat Substrate SufI Is Critical for the Ability of *Yersinia pseudotuberculosis* To Cause Systemic Infection. *Infect Immun* 85.
85. Typas A, Banzhaf M, Gross CA, Vollmer W (2011) From the regulation of peptidoglycan synthesis to bacterial growth and morphology. *Nat Rev Microbiol* 10: 123–136. <https://doi.org/10.1038/nrmicro2677> PMID: 22203377
86. Lange R, Hengge-Aronis R (1994) The *nlpD* gene is located in an operon with *rpoS* on the *Escherichia coli* chromosome and encodes a novel lipoprotein with a potential function in cell wall formation. *Mol Microbiol* 13: 733–743. PMID: 7997184
87. Bernhardt TG, de Boer PA (2003) The *Escherichia coli* amidase AmiC is a periplasmic septal ring component exported via the twin-arginine transport pathway. *Mol Microbiol* 48: 1171–1182. PMID: 12787347

88. Uehara T, Parzych KR, Dinh T, Bernhardt TG (2010) Daughter cell separation is controlled by cytokinetic ring-activated cell wall hydrolysis. *EMBO J* 29: 1412–1422. <https://doi.org/10.1038/emboj.2010.36> PMID: 20300061
89. Tsang MJ, Yakhnina AA, Bernhardt TG (2017) NlpD links cell wall remodeling and outer membrane invagination during cytokinesis in *Escherichia coli*. *PLoS Genet* 13: e1006888. <https://doi.org/10.1371/journal.pgen.1006888> PMID: 28708841
90. Gibson UE, Heid CA, Williams PM (1996) A novel method for real time quantitative RT-PCR. *Genome Res* 6: 995–1001. PMID: 8908519